

# Deep Demosaicing for Edge Implementation

R. Ramakrishnan<sup>1</sup>, J. Shangling<sup>2</sup>, and V. Patrovi Nia<sup>1</sup>

<sup>1</sup> Huawei Technologies, Naoh's Ark Lab, Montreal Research Centre.

<sup>2</sup> Huawei Technologies, Kirin Solution, HiSilicon Shanghai.

**Abstract.** Most digital cameras use sensors coated with a Color Filter Array (CFA) to capture channel components at every pixel location, resulting in a mosaic image that does not contain pixel values in all channels. Current research on reconstructing these missing channels, also known as *demosaicing*, introduces many artifacts, such as *zipper effect* and *false color*. Many deep learning demosaicing techniques outperform other classical techniques in reducing the impact of artifacts. However, most of these models tend to be over-parametrized. Consequently, edge implementation of the state-of-the-art deep learning-based demosaicing algorithms on low-end edge devices is a major challenge. We provide an exhaustive search of deep neural network architectures and obtain a pareto front of Color Peak Signal to Noise Ratio (CPSNR) as the performance criterion versus the number of parameters as the model complexity that beats the state-of-the-art. Architectures on the pareto front can then be used to choose the best architecture for a variety of resource constraints. Simple architecture search methods such as exhaustive search and grid search requires some conditions of the loss function to converge to the optimum. We clarify these conditions in a brief theoretical study.

**Keywords:** Deep Learning · Demosaicing · Edge Computing · Network Architecture Search

## 1 Introduction

Deep Learning is changing lives on a day to day basis. Breakthrough models on machine translation, self-driving cars, Alpha Go, etc have shown game-changing breakthroughs. However, most of these models are highly over-parametrised for a variety of reasons ranging from the increase of computational power to the lack of domain expertise. Subsequently, deploying these models on severely constrained edge devices is not straightforward.

Overparametrization of deep models can have an impact in their deployment for variety of applications. For instance, model size could adversely affect the real-time updates in mobile phones implementation. Moreover, the training and inference time raises for a large model. For instance, ResNet152 takes 1.5 weeks to train on the ImageNet dataset using one Nvidia TitanX GPU [4]. In terms of hardware, much of the impact of such models is in the energy consumption. As an example, Dynamic Random Access Memory (DRAM) consumes most of the energy at inference. Therefore, it is imperative to reduce the model size [3].

As an alternative most of deep models are stored on the cloud rather than edge devices to overcome many of edge implementation drawbacks and perform computation on the cloud server. However, the cons far outweigh the pros, especially in terms of security, or the latency in transferring the data from cloud and vice-versa. Therefore, most of the models need to be stored and computed on the edge in real applications.

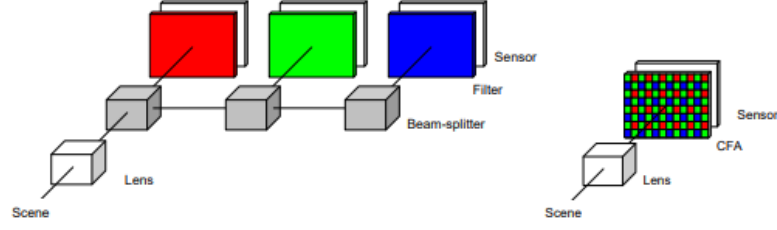
The success of deep learning models has been proven in many high-level vision tasks such as image classification and object detection. However, deep learning solutions are less explored for low-level vision problems where the edge implementation is an obligation. Previous work shows the effectiveness on other low-level vision problems such as image denoising and image demosaicing [18]. Here we explore various architectures for demosaicing, with the aim of finding suitable models for deployment on the edge. It is imperative to make use of models that can be stored on edge devices.

The paper is structured as follows: Section 2 introduces the demosaicing problem and the various techniques to solve it, Section 3 introduces the architecture search technique used, Section 4 introduces the search methodology for architecture search and establishes the basic theoretical conditions for exhaustive search and grid search, and Section 5 performs architecture search for demosaicing.

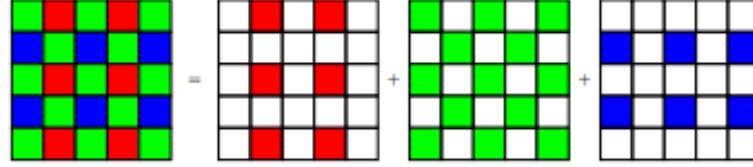
## 2 Demosaicing

Image demosaicing involves interpolating full-resolution images from incomplete color samples produced by an image sensor. Limitations in camera sensor resolution and sensitivity leads to the problem of mosaicing. For a digital camera to capture or produce a full color image, it uses sensors to detect all 3 colors (RGB) at every pixel location. One of the ways this is done involves using a beam-splitter to project the image onto three separate sensors, see Figure 1, one for each color (RGB). Color filters are placed in front of each sensor to filter specific wavelengths such that three full-channel color images are obtained. This is a costly process that is generally used in scientific-grade microscopes. Most digital cameras, on the other hand, make use of just one sensor coated with a Color Filter Array (CFA). In this system, one color component is captured at every pixel location and the missing channels are reconstructed. The resultant image is often called a mosaic image, derived from the CFA’s mosaic pattern. This mosaic image is then subjected to software-based interpolation, resulting in a full-resolution image; a process is termed *demosaicing*.

Various existing CFA patterns are currently used, with the Bayer CFA being the most commonly used approach for mosaicing. The Bayer CFA measures the green image on *quincunx* grid, and the red/blue on the rectangular grids (Figure 2). The green channel has higher sampling because the human retina has a higher sensitivity toward the green wavelength.



**Fig. 1.** Optical path for multichip and single chip digital camera, borrowed from [6]



**Fig. 2.** Bayer Pattern in single chip digital cameras, borrowed from [6]

Let  $I^{CFA} : \mathbb{Z}^2 \rightarrow \mathbb{Z}$  denote an  $M \times N$  Bayer CFA image. If we consider the sampling pattern shown in Figure 2, then the mosaic image is as follows:

$$I(i, j) = \begin{cases} R_{i,j} & \text{for } i \text{ odd and } j \text{ even,} \\ B_{i,j} & \text{for } i \text{ even and } j \text{ odd,} \\ G_{i,j} & \text{Otherwise,} \end{cases} \quad (1)$$

where  $R_{i,j}$ ,  $G_{i,j}$ ,  $B_{i,j}$  includes values between 0 and 255. To estimate the missing two missing channels for each pixel location using demosaicing,

$$\hat{I}(i, j) = \begin{cases} (R_{i,j}, \hat{B}_{i,j}, \hat{G}_{i,j}) & \text{for } i \text{ odd and } j \text{ even,} \\ (\hat{R}_{i,j}, B_{i,j}, \hat{G}_{i,j}) & \text{for } i \text{ even and } j \text{ odd,} \\ (\hat{R}_{i,j}, \hat{B}_{i,j}, G_{i,j}) & \text{Otherwise,} \end{cases} \quad (2)$$

where  $\hat{R}_{i,j}, \hat{G}_{i,j}, \hat{B}_{i,j}$  are the estimates for the channels at each pixel location.

Demosaicing approaches are divided into various categories: 1. Edge-sensitive methods, 2. Directional interpolation and decision methods, 3. Frequency domain approaches, 4. Wavelet-based methods, 5. Statistical reconstruction techniques, and 6. Deep learning [9]. Early studies in bi-linear/bi-cubic [20] and spline interpolation make use of single-channel interpolation techniques that treat each channel separately, without using the inter-channel information and correlation. For instance, bi-linear interpolation computes the red value of a non-red pixel as the average of the 2/4 adjacent red pixels; this method is then repeated with the

blue and green pixels. Many comparatively advanced algorithms use the results of bi-linear interpolation as an initial baseline. These algorithms make use of a weighted average of the neighboring pixels to fill the missing channel values.

Recently, neural network approaches like convolutional neural networks (CNN) have been effectively used for joint denoising and demosaicing [2]. This method downsamples the mosaiced image using multiple convolutions and computes the residual at lower resolution; this is further concatenated with the input mosaic image. The final output is then calculated using another group of convolutions at full resolution to reconstruct the full resolution image (Figure 3a). Studies [16] have also used Deep Residual Learning for image demosaicing. This neural network uses a two-stage architecture: 1) the first step recovers an intermediate result of the Green and Red/Blue channel separately as a guiding prior to use as input for the second stage, 2) the final demosaiced image is reconstructed (Figure 3b). These approaches solved the Bayer demosaicing.

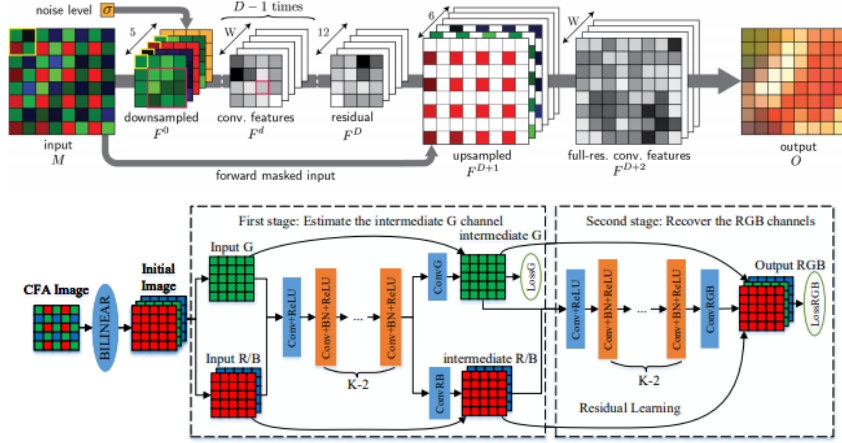


**Fig. 3.** Architecture proposed in [2] (top panel) versus [16] (bottom panel).

The DMCNN-VD [15] architecture (Figure 4) consists of a deep network that uses same dimensions for the input and output layers. They use the Bayer CFA mosaic layer and 20 blocks (CNN, BN, SELU), instead of the 3 layers in the DMCNN model.

## 2.1 Artifacts

The major disadvantage of demosaicing algorithms is its propensity to introduce unwanted artifacts into resulting images. A previous study shows that bi-linear interpolation of mosaic images results in various structural errors [5], such as the two homogeneous areas with 2 gray levels low and high intensity ( $L$  and  $H$ ,

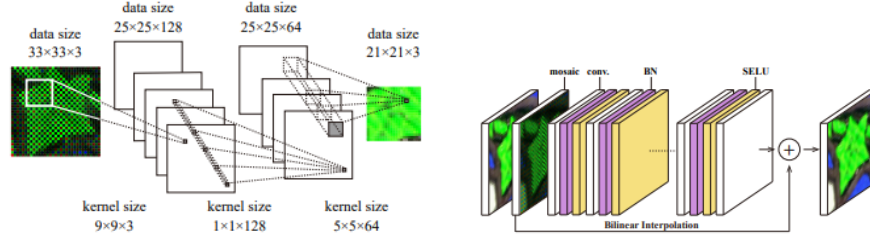


**Fig. 4.** DMCNN (left) and DMCNN-VD (right) architectures introduced in [15].

$L < H$ ) represented in Figure 5. Another artifact introduced is the mismatch in the green channel and blue/red channel intensity.

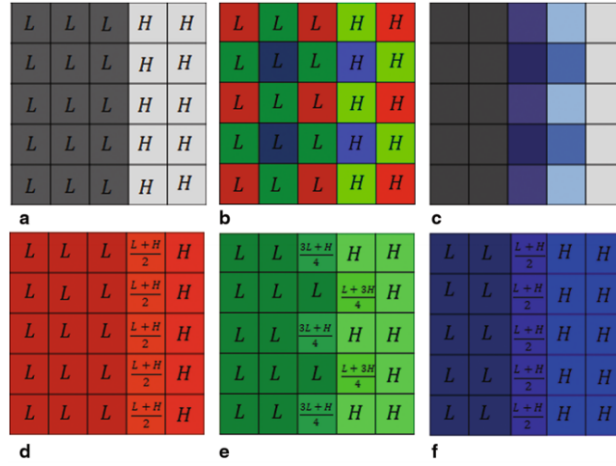


**Fig. 5.** a: Gray image, b: CFA of a, c: Bilinear interpolation result, d e f: interpolation in color plane, borrowed from [21].

These 2 artifacts are generalized as *zipper effect* and *false color*. The zipper effect is an abrupt or sudden change in intensity over the neighboring pixels, generally seen along the edges (Figure 6a). False colors (Figure 6b), on the other hand, are pseudo-colors that are not an accurate representation of the original image. This generally occurs due to inconsistencies in color channels of the original mosaic image. Both these effects are categorized as misguidance color artifacts, generated as a result of wrong interpolation direction. Interestingly, these artifacts are observed even when the interpolation direction is appropriate. However, the effects in this case are less evident when compared to misguided color artifacts.



**Fig. 6.** Zipper Effect and False color - Original image and bilinear interpolated image. [5]

## 2.2 Performance Evaluation

A common demosaicing approach is to capture the ground truth images using a professional 3-sensor camera, convert them into a mosaic format using Bayer CFA, interpolate using a demosaicing algorithm, and then compare the results with the ground truth image. Widely used performance criteria are mean Squared Error (MSE) or equivalent Peak Signal to Noise Ratio (PSNR). The Kodak / McMaster [19] dataset is generally used as a baseline because of the realistic scenes and varied complexities. The MSE in each color plane is defined as,

$$\text{MSE}(k) = \frac{1}{MN} \sum_{i=1}^M \sum_{j=1}^N \{\hat{I}_k(i, j) - I_k(i, j)\}^2, \quad (3)$$

where  $\hat{I}_k(i, j)$  is the predicted color component pixel and  $I_k(i, j)$  is the original pixel color component.

Another measure is the Color Mean Squared Error (CMSE) ([9]) which averages over the color channel as well,

$$\text{CMSE}(I, \hat{I}) = \frac{1}{3MN} \sum_{k \in \{R, G, B\}} \sum_{i=1}^M \sum_{j=1}^N \{\hat{I}_k(i, j) - I_k(i, j)\}^2, \quad (4)$$

The peak signal to noise ratio (PSNR) is defined as,

$$\text{PSNR}(k) = 10 \log_{10} \left( \frac{R^2}{\text{MSE}} \right), \quad (5)$$

where R is 1.0 (for float datatype), R is 255 (for integer datatype).

The Color Peak Signal to Noise Ratio (CPSNR) is computed by replacing MSE with CMSE. The higher the PSNR value, better is the quality of the demosaiced image.

## 3 Architecture Search

For the exhaustive search of architectures, we made use of various parameters chosen based on state-of-the-art models to obtain the pareto front between nega-

tive CPSNR as the loss and the number of parameters as the model complexity. The various hyper-parameters for exhaustive search were mostly discrete and are as follows:

1. The use of depthwise separable convolutions [13], similar to MobileNet V2 architecture [11], over the traditional convolutional layers as per the state-of-the-art models.
2. The number of filters used in the models (16, 32, 64, 128 and 256).
3. Number of blocks, each block consists of sets of i) depthwise separable ii) normal convolutions, and iii) activation chosen from (3,5,7).
4. We use a constant kernel size of  $3 \times 3$  since much of the hardware has shown to be optimized for this convolution [8].
5. The length of skip connections (1,2).
6. The use of cosine annealing [7] or a fixed learning rate.

To make the comparisons fair, we ran each model for 500 epochs and retrained the state-of-the-art architecture in this new setting.

Some of the reasoning behind choosing the search space is as follows:

1. Primary reason for choosing this range of filter and block values was to obtain networks that have a smaller number of parameters and FLOPs as the current state-of-the-art networks. The filters and block size dominate the parameter density in a network. We defined an upper bound based on this setting.
2. Motivated from [8], choosing equal channel width minimizes memory access cost (MAC). Hence, we retained the same channel width across all the layers in the network.
3. Furthermore, [8] computed the relative costs of using group convolution, so we used the depth-wise convolution in all the layers.
4. Moreover, for deployment in edge devices, various restrictions are placed based on the platform for inference. In this problem, the model size, the number of FLOPs and MAC play a key role in inference time. For instance, the largest model we have has around  $7 \times 10^5$  parameters and  $5.2 \times 10^6$  multiplication FLOPs. Deploying such a model would have severe consequences in the overall usability of the edge device.
5. We chose a lower bound on the number of filters, around the region, based on the smallest state-of-the-art model, i.e. DMCNN [15].
6. We used point-wise convolutions to avoid the use of fully-connected layers as the last layer, and therefore reduce the model size.

Our goal in this study is to explore architectures that improves the state of the art models by using fewer number of parameters and maintaining reasonable accuracy for edge implementation.

## 4 Methodology and Theory

Most of the state-of-the-art methods for neural architecture search focus on reinforcement learning and genetic algorithm. The work that first led to the

prominence of AutoML and NAS to the outside world; [22] uses recurrent neural network to generate model descriptions of artificial neural networks, followed by reinforcement learning to maximize the accuracy with respect to a known validation set. Another study [23] created a method for learning transferable architectures for scalable image recognition. They use a small dataset like the CIFAR-10 to search for a network architecture. Once this was obtained, they transfer this architecture block to a larger dataset like ImageNet. Efficient Neural Architecture Search (ENAS) [10] is a follow up for automatic model design. In ENAS, a controller is able to find various neural network architectures by searching through an optimal sub-graph of a large computational graph. All of these methods are computationally expensive and require many model evaluations. [12] proposes evolving neural architectures inspired by biological evolution. Our approach is to use the expert knowledge in the field and design a meaningful search space where exhaustive search is a feasible tool.

Bayesian optimization is also a common practice for optimizing architectures. However, Bayesian optimization suites continuous parameter tuning such as learning rate, cosine annealing period, regularization constant etc. Sometimes even ordinal parameters such as filter size, number of training iteration, etc is also tuned using Bayesian optimization as a heuristic method. We use Bayesian optimization only on learning rate and regularization constant on the pareto front architectures to improve the the search further.

Neural architecture search is a discrete optimization problem. Here we used an exhaustive search over a small space, where the convergence to the optimum in the designed space is trivial and independent of the loss function, because all points are evaluated. However, most of these neural architecture search techniques are motivated by a very large design space. Here we showed that as soon as the designed space gets large, even very simple methods such as exhaustive search and grid search, require some minimal properties of the loss function to convergence to the optimum.

Exhaustive search and grid search techniques are common optimization methods that rely only on function evaluation. Therefore, it is counter-intuitive that finding the optimum point using these techniques may require some mathematical assumptions about the search space, or the objective function. Motivated from the derivative-free optimization theory, we aim at clarifying some minimal conditions that the exhaustive search and grid search converges to the optimum.

Let's set the notation first. Here we denote a vector using bold  $\theta$  and an element of the this vector using unbold  $\theta$ . The search space can be a mix of continuous or discrete parameters and denoted by  $\Theta$ . Suppose a neural network is uniquely defined by its hyperparameters embedded in  $\theta \in \Theta$ . Note that the complexity of each network might differ. Complexity may be defined as the number of parameters of the network, inference delay, training time, etc. Often the objective is to discover the neural network with minimum loss (or maximum accuracy) on a fixed validation set. Let's denote the validation loss of the neural network with  $L(\theta)$  and its complexity  $C(\theta)$ . It is preferable to minimize  $L(\theta)$  and  $C(\theta)$  at the same time, i.e. between two neural networks with the same validation



loss  $L(\cdot)$ , the neural network with smaller complexity  $\mathcal{C}(\cdot)$  is preferred. To simplify the theoretical analysis we assume that  $\mathcal{C}(\cdot)$  is fixed and focus on minimizing the validation loss function  $L(\cdot)$  regardless of  $\mathcal{C}(\cdot)$ . In the context of demosaicing  $L(\cdot)$  is the negative CPSNR and  $\mathcal{C}(\cdot)$  is the number of model parameters.

Assume the minimum exist within the search space  $\Theta$

$$\operatorname{argmin}_{\theta \in \Theta} L(\theta) \neq \emptyset \quad (6)$$

Let's define the exhaustive search algorithm to minimize  $L(\cdot)$  as

1. Enumerate:  $\{\theta_0, \theta_1, \dots, \theta_K\}$ .
2. Initialize:  $k = 0, \theta^* = \theta_0, L^* = L(\theta_0)$ .
3. Evaluate  $L(\theta_{k+1})$ .
4. If  $L(\theta_{k+1}) < L^*$ , then update  $\theta^* = \theta_{k+1}, L^* = L(\theta_{k+1})$ .
5. If  $k < K$  then  $k = k + 1$  go to 3, otherwise end.

It is trivial that after iterating the algorithm  $K$  iterations, the global minimum of the objective function is obtained  $(\theta^*, L(\theta^*))$ , for simplicity of notation we may denote  $(\theta^*, L^*)$  where

$$\begin{aligned} \theta^* &= \operatorname{argmin}_{\theta \in \Theta} L(\theta), \\ L^* &= \min_{\theta \in \Theta} L(\theta). \end{aligned}$$

Convergence to the optimum requires no restriction on the loss function  $L(\cdot)$  except the existence of the minimum (6). However, if the algorithm is iterated only  $k < K$  iterations there is no guarantee of convergence to the minimum.

Often the cardinality  $|\Theta| = K$  is a large value because in real scenario a grid search on the hyperparameter vector  $\theta$  is implemented, where the search becomes NP-hard,  $K = \mathcal{O}(e^d)$  where  $d = \dim(\theta)$ , and the algorithm is run only  $k < K$  iterations depending on computation budget.

In the following sections we explore under what conditions the exhaustive search convergence is assured. Suppose the search space is large but is countable,  $K = \infty$ . Infinitely many evaluations requires more conditions on  $L(\cdot)$ . For simplicity of the notation we may assume  $\Theta \subset \mathbb{R}^d$  where  $d = \dim(\theta)$ . Suppose the minimum argument and the objective value at iteration  $k$  of exhaustive search is denoted by  $(\theta_k^*, L_k^*)$

**Theorem 1.** *If  $\Theta$  is dense and  $L(\cdot)$  is continuous, the exhaustive search converges to the minimum value*

$$\lim_{k \rightarrow \infty} L_k^* = L^*.$$

*Proof.* Take the optimal solution  $\theta^* \in \Theta$  and because  $L(\cdot)$  is continuous and  $\Theta$  is dense

$$\exists \delta > 0, \theta_k \in \Theta_k \text{ where } \|\theta_k - \theta^*\| < \delta, |L(\theta_k) - L(\theta^*)| < \epsilon,$$

or equivalently  $L(\theta_k) < L(\theta^*) + \epsilon$ . On the other hand  $\forall k, L(\theta^*) \leq L(\theta_k^*) \leq L(\theta_k)$  and by definition  $L^* = L(\theta^*)$ ,  $L_k^* = L(\theta_k^*)$ , so

$$L^* \leq L_k^* \leq L(\theta_k) \leq L^* + \epsilon,$$

so

$$\lim_{k \rightarrow \infty} L_k^* = L^*.$$

**Theorem 2.** *If  $\Theta$  is compact and  $\theta^* = \operatorname{argmin}_{\theta \in \Theta} L(\theta)$  is unique, the exhaustive algorithm converges to the unique minimum.*

*Proof.*  $\forall k, \theta_k \in \Theta$  which is compact, so there is a subsequence that converges to  $\theta_k^*$ , call it  $\theta_{ik}^*$

$$\lim_{k \rightarrow \infty} \lim_{i \rightarrow \infty} \theta_{ik}^* = \tilde{\theta}.$$

By continuity of  $L(\cdot)$

$$\lim_{k \rightarrow \infty} \lim_{i \rightarrow \infty} L(\theta_{ik}^*) = L(\tilde{\theta}),$$

but from Theorem 1 we know  $\lim_{k \rightarrow \infty} L(\theta_k^*)$ , therefore  $\tilde{\theta} \in \Theta$ . From the uniqueness of the minimum  $\tilde{\theta} = \theta^*$ .

The convergence of exhaustive search relies on the continuity of  $L(\cdot)$ . It is easy to construct cases while exhaustive search fails to converge if  $L(\cdot)$  is non-continuous, for more details see [1]. Although exhaustive search is the first tool to explore the space for discrete space, in a continuous space exhaustive search is infeasible. Therefore optimizing over a continuous parameter such as learning rate, annealing rate, regularization constant, etc requires other tools. Bayesian optimization [14] is often used and some open source packages are available [17]. However, still the most s of the optimization tool to tune a continuous parameter is the grid search.

Grid search on multiple variables is cumbersome, because as the dimension of the search variable  $d$  gets large, the evaluation set is  $\mathcal{O}(n^d)$ . Multivariate grid search algorithm over the set  $\prod_{i=1}^d [a_i, b_i] \subset \mathbb{R}^d$  is

1. Initialize number of grid evaluation  $n \in \mathbb{N}$
2. Set the step size  $\delta_i = \frac{b_i - a_i}{n-1}, i = 1, \dots, d$ .
3. Create the grid search space with step iteration  $j$

$$\Theta_n = \{\theta \mid \theta = l_i + j\delta_i, j = 0, \dots, n-1, i = 1, \dots, d\}$$

4. Evaluate the objective function  $L(\cdot)$  for all  $n^d$  grid points  $\theta \in \Theta_n$
5. Find the grid search solution  $(\theta_n^*, L_n^*)$  where

$$\theta_n^* = \operatorname{argmin}_{\theta \in \Theta_n} L(\theta), \quad L_n^* = \min_{\theta \in \Theta_n} L(\theta).$$

Grid search on  $d$  variables is NP-hard, so it is commonly implemented only on one element of the vector  $\theta$  while keeping the other elements fixed to certain

values. Therefore, it makes more sense to explore the convergence of the grid search on a univariate variable  $\theta$ .

Suppose the continuous univariate parameter  $\theta \in [a, b]$  that achieves its minimum at  $(\theta^*, L^*)$ . The univariate parameter  $\theta$  is a continuous element, such as the learning rate, an element of the vector  $\boldsymbol{\theta}$ , in which the vector  $\boldsymbol{\theta}$  fully determines the neural network.

The grid search convergence result relies on creating a nearly dense set  $\Theta_n$  by choosing a large number of grid evaluation  $n$ . The convergence also depends  $L(\theta)$  to be Lipschitz continuous, i.e.

$$\forall \theta, \theta' \in [a, b], |L(\theta) - L(\theta')| \leq M|\theta - \theta'|,$$

where  $M$  is the Lipschitz constant.

**Theorem 3.** *Suppose  $L(\cdot)$  is Lipschitz continuous on  $\theta \in [a, b]$  and a grid search is run over  $n$  grids to create  $\Theta_n$  with step size  $\delta$ , then*

$$L_n^* - \frac{M\delta}{2} \leq L^*$$

*Proof.* Suppose  $\theta^* \in \Theta$ , take  $\theta_n \in \Theta_n$  as a grid search candidate. For any point in the grid  $\Theta_n$ , define the closest point to  $\theta^*$  in the grid space  $\theta_n^* = \operatorname{argmin}_{\theta_n \in \Theta_n} |\theta_n - \theta^*|$ . The distance between two consecutive points is  $\delta$ , so  $|\theta_n^* - \theta^*| \leq \frac{\delta}{2}$ . By the Lipschitz continuity of  $L(\cdot)$

$$|L(\theta_n^*) - L(\theta^*)| \leq M|\theta_n^* - \theta^*| \leq \frac{M\delta}{2}$$

which immediately follows

$$L_n^* - \frac{M\delta}{2} \leq L^*.$$

Theorem 3 means for a finite  $n$ ,  $L_n^*$  may never reach to the true minimum  $L^*$  as  $L^* \leq L_n^*$ , but improves fast as  $\delta$  gets smaller by evaluating smaller step size or equivalently by increasing the number of evaluations  $n$ ; the lower-bound improves of  $\mathcal{O}(n^{-1})$ .

## 5 Application

We first describe the dataset that was used for our experiments and elaborate on the results obtained.

Flickr500 data is used by [15] to generate around 3.5 million patches. The authors chose the images with some criteria such as i) the images were colorful to obtain the proper color distributions of real world, ii) high-frequency patterns in the images and iii) they are of a high-quality. However, there were some key points missing in the description to re-generate the exact results such as

1. Specifications on exactly how the patches were generated from the original Flickr 500 images (related to the stride etc while cropping the patches).

2. Specifications on how to apply the Bayer CFA for creating the sample mosaic image.

Therefore, we made some assumptions to these key points while generating our data.

1. We generated random patches of  $32 \times 32 \times 3$  to obtain approximately 1.5 million images from the 500 images. Since the method is not specified, we used random points in the image and extracted patches from the random points. 1382400 images were used for the training set and 153600 images for the validation set. Note: In the paper, they use patches of size  $33 \times 33 \times 3$  but we use  $32 \times 32 \times 3$  because the training is much faster on GPU due to tiling, and due to the dimensions being a power of 2.
2. The Bayer CFA generation is also based on the python package. We used the default setting of *RGGB* and filled the missing channels with zeros to maintain the channel dimensions.
3. All the results in the section were calculated against the McMaster dataset (MCM) containing 18 photos (58000 patches created), and the Kodak images containing 24 photos (78408 patches created).

The pareto front of our exhaustive search is shown in Figure 7. The  $y$ -axis represents the validation loss  $L(\cdot)$  which indicates the negative CPSNR and the  $x$ -axis represents the model complexity  $\mathcal{C}(\cdot)$  which is the total number of parameters in the neural model. The standard error for each experiment is calculated and they are comparable so produce a similar prediction interval.

Most of the architectures in the search space outperform the current state-of-the-art as in Figure 7 in a similar setting, see also Table 1. Furthermore, the total number of parameters in the current state-of-the-art is approximately  $7 \times 10^5$ . Architectures on the pareto front keep the the same accuracy while reducing the number of parameters to much fewer. In our search the effect of cosine annealing was not obvious, although it did improve the results. Further tuning on the cycle rate is needed to see the real effect. The ResNet skip connections length made a difference in the overall convergence of the models. The skip length of 2 blocks worked better than 1. All the experiments were implemented in the same setting and ran for 500 epochs each.

Some of the models on the pareto front are shown in the table below in comparison to the current state-of-the-art models for the MCM dataset. Once the initial search was completed, the models from the pareto front architectures were fed through a Bayesian optimizer using the ORION package [17]. The learning rate and regularization constant for  $L_2$  regularization were optimized further using Bayesian optimization. Figure 7 indicates further improvement over the initial CPSNR obtained with a fixed learning rate  $10^{-4}$  and regularization constant  $10^{-8}$ , so Bayesian optimization is recommended as an extra step after architecture search.

In our experiments, the PSNR was calculated separately for each image in the test dataset; the final CPSNR value was the mean of all the PSNRs of all images in the dataset.

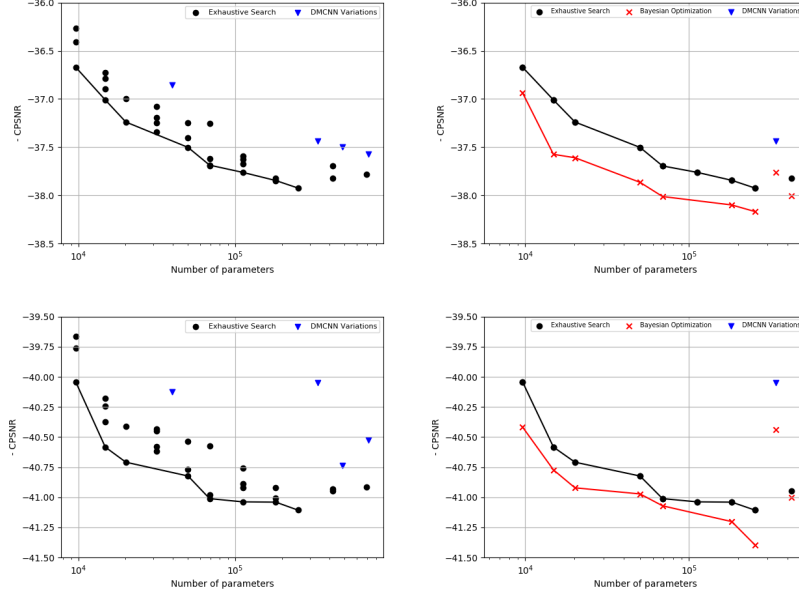


**Fig. 7.** Pareto front of MCM dataset 18 photos with standard error 0.53 (top panels) compared to and Kodak dataset 24 photos standard error 0.66 (bottom panels). Left panels is exhaustive search versus right Bayesian Optimization of learning rate and regularization constant implemented on pareto architectures.

## 6 Conclusion

Our designed space with a simple exhaustive search outperforms the state of the art and brings a range of loss versus complexity for edge implementation with varying resource constraints. Although in most of architecture search, the number of evaluations and complex search algorithm implementation is a bottleneck, here we showed using the expert domain knowledge overcomes these drawbacks and a simple exhaustive search becomes an effective search tool. Here we only focused on demosaicing as an example of a low-vision problem where edge implementation is an obligation. We wonder whether a similar approach is useful in edge implementation of other low vision problems.

Overall, our architecture search demonstrates significant improvements over the state-of-the-art in terms of negative CPSNR as the loss and the number of parameters as the model complexity criterion. Bayesian optimization can be used further for the pareto efficient architectures to improve the results even further. The explored architectures can be used in various resource constrained environments upon requirements while complexity versus performance is the main challenge. These architectures can be used also as a baseline for more complex search such as NAS, ENAS, using reinforcement learning or genetic algorithm.

Model	no of blocks	skip length	L(.)	Standard Error	C(.)
<b>64 filter</b>	<b>20</b>	<b>20</b>	-37.58	<b>0.66</b>	<b>710275</b>
64 filter	15	15	-37.51	0.62	487171
64 filter	10	10	-37.45	0.64	338435
256 filter	5	2	-37.74	0.69	692239
256 filter	3	2	-37.77	0.68	420879
128 filter	7	2	-37.94	0.67	252431
128 filter	5	2	-37.82	0.69	182287

**Table 1.** The negative CPSNR denoted by  $L(\cdot)$  versus the number of parameters denoted by  $C(\cdot)$  for few architectures of the search space on the MCM dataset. The first line in bold shows the state-of-the-art.

Simple theoretical study suggests continuity of the loss function, and compactness of the search space is required so that exhaustive search and grid search converge to the optimum.

## Acknowledgement

We want to ccknowledge Heng Liao and Yanhui Geng for their support to work on this project. We appreciate the help of Huawei media research lab of Japan. We would like to declare our gratitude to Charles Audet and Sebastien Le Digabel who introduced us the theory behind the derivative-free optimization.

## References

1. Audet, C., Hare, W.: Derivative-free and blackbox optimization. Springer (2017)
2. Gharbi, M., Chaurasia, G., Paris, S., Durand, F.: Deep joint demosaicking and denoising. ACM Trans. Graph. **35**(6), 191:1–191:12 (Nov 2016). <https://doi.org/10.1145/2980179.2982399>, <http://doi.acm.org/10.1145/2980179.2982399>
3. Han, S., Liu, X., Mao, H., Pu, J., Pedram, A., Horowitz, M.A., Dally, W.J.: Eie: Efficient inference engine on compressed deep neural network. SIGARCH Comput. Archit. News **44**(3), 243–254 (Jun 2016). <https://doi.org/10.1145/3007787.3001163>, <http://doi.acm.org/10.1145/3007787.3001163>
4. Han, S., Pool, J., Tran, J., Dally, W.J.: Learning both weights and connections for efficient neural networks. CoRR **abs/1506.02626** (2015), <http://arxiv.org/abs/1506.02626>
5. Lanlan Chang, Y.P.T.: Hybrid color filter array demosaicking for effective artifact suppression. Journal of Electronic Imaging **15**, 15 – 15 – 17 (2006). <https://doi.org/10.1117/1.2183325>, <https://doi.org/10.1117/1.2183325>
6. Li, X., Gunturk, B.K., Zhang, L.: Image demosaicing : A systematic survey (2007)
7. Loshchilov, I., Hutter, F.: SGDR: stochastic gradient descent with restarts. CoRR **abs/1608.03983** (2016), <http://arxiv.org/abs/1608.03983>

8. Ma, N., Zhang, X., Zheng, H., Sun, J.: Shufflenet V2: practical guidelines for efficient CNN architecture design. CoRR **abs/1807.11164** (2018), <http://arxiv.org/abs/1807.11164>
9. Menon, D., Calvagno, G.: Color image demosaicking: An overview. Image Commun. **26**(8-9), 518–533 (Oct 2011). <https://doi.org/10.1016/j.image.2011.04.003>, <http://dx.doi.org/10.1016/j.image.2011.04.003>
10. Pham, H., Guan, M.Y., Zoph, B., Le, Q.V., Dean, J.: Efficient neural architecture search via parameter sharing. CoRR **abs/1802.03268** (2018), <http://arxiv.org/abs/1802.03268>
11. Sandler, M., Howard, A.G., Zhu, M., Zhmoginov, A., Chen, L.: Inverted residuals and linear bottlenecks: Mobile networks for classification, detection and segmentation. CoRR **abs/1801.04381** (2018), <http://arxiv.org/abs/1801.04381>
12. Shafiee, M.J., Mishra, A., Wong, A.: Deep learning with darwin: evolutionary synthesis of deep neural networks. Neural Processing Letters **48**(1), 603–613 (2018)
13. Sifre, L., Mallat, S.: Rigid-motion scattering for texture classification. CoRR **abs/1403.1687** (2014), <http://arxiv.org/abs/1403.1687>
14. Snoek, J., Larochelle, H., Adams, R.P.: Practical bayesian optimization of machine learning algorithms. In: Pereira, F., Burges, C.J.C., Bottou, L., Weinberger, K.Q. (eds.) Advances in Neural Information Processing Systems 25, pp. 2951–2959. Curran Associates, Inc. (2012), <http://papers.nips.cc/paper/4522-practical-bayesian-optimization-of-machine-learning-algorithms.pdf>
15. Syu, N., Chen, Y., Chuang, Y.: Learning deep convolutional networks for demosaicing. CoRR **abs/1802.03769** (2018), <http://arxiv.org/abs/1802.03769>
16. Tan, H., Xiao, H., Lai, S., Liu, Y., Zhang, M.: Deep residual learning for image demosaicing and blind denoising (08 2018). <https://doi.org/10.13140/RG.2.2.11048.62725>
17. Tsirigotis, C., Bouthillier, X., Corneau-Tremblay, F., Henderson, P., Askari, R., Lavoie-Marchildon, S., Deleu, T., Suhubdy, D., Noukhovitch, M., Bastien, F., et al.: Orfon: Experiment version control for efficient hyperparameter optimization (2018)
18. Xie, J., Xu, L., Chen, E.: Image denoising and inpainting with deep neural networks. In: Pereira, F., Burges, C.J.C., Bottou, L., Weinberger, K.Q. (eds.) Advances in Neural Information Processing Systems 25, pp. 341–349. Curran Associates, Inc. (2012), <http://papers.nips.cc/paper/4686-image-denoising-and-inpainting-with-deep-neural-networks.pdf>
19. Yu, K., Wang, C., Yang, S., Lu, Z., Zhao, D.: An effective directional residual interpolation algorithm for color image demosaicking. Applied Sciences **8**, 680 (04 2018). <https://doi.org/10.3390/app8050680>
20. Yu, W.: Colour demosaicking method using adaptive cubic convolution interpolation with sequential averaging. IEE Proceedings - Vision, Image and Signal Processing **153**(5), 666–676 (Oct 2006). <https://doi.org/10.1049/ip-vis:20050281>
21. Zhen, R., Stevenson, R.L.: Image demosaicing. Springer International Publishing pp. 15 – 15 – 17 (2015). <https://doi.org/https://doi.org/10.1007/978-3-319-09363-5-2>
22. Zoph, B., Le, Q.V.: Neural architecture search with reinforcement learning. CoRR **abs/1611.01578** (2016), <http://arxiv.org/abs/1611.01578>
23. Zoph, B., Vasudevan, V., Shlens, J., Le, Q.V.: Learning transferable architectures for scalable image recognition. CoRR **abs/1707.07012** (2017), <http://arxiv.org/abs/1707.07012>